PHOTONICS Research

Controlling the collective radiative decay of molecular ions in strong laser fields

Hongqiang Xie,[1,2,†] Hongbin Lei,[2,†] Guihua Li,[2,3] Jinping Yao,[4] Qian Zhang,[2] Xiaowei Wang,[2] Jing Zhao,[2] Zhiming Chen,[1] Ya Cheng,[5] and Zengxiu Zhao[2,*]

[1]School of Science, East China University of Technology, Nanchang 330013, China
[2]Department of Physics, National University of Defense Technology, Changsha 410073, China
[3]School of Science, East China Jiaotong University, Nanchang 330013, China
[4]State Key Laboratory of High Field Laser Physics and CAS Center for Excellence in Ultra-intense Laser Science, Shanghai Institute of Optics and Fine Mechanics, Chinese Academy of Sciences (CAS), Shanghai 201800, China
[5]State Key Laboratory of Precision Spectroscopy, East China Normal University, Shanghai 200062, China
*Corresponding author: zhao.zengxiu@gmail.com

Received 23 June 2021; revised 10 August 2021; accepted 16 August 2021; posted 17 August 2021 (Doc. ID 434378); published 24 September 2021

Molecular ions, produced via ultrafast ionization, can be quantum emitters with the aid of resonant electronic couplings, which makes them the ideal candidates to study strong-field quantum optics. In this work, we experimentally and numerically investigate the necessary condition for observing a collective emission arising from macroscopic quantum polarization in a population-inverted N_2^+ gain system, uncovering how the individual ionic emitters proceed into a coherent collection within hundreds of femtoseconds. Our results show that for a relatively high-gain case, the collective emission behaviors can be readily initiated for all the employed triggering pulse area. However, for a low-gain case, the superradiant amplification is quenched since the building time of macroscopic interionic quantum coherence exceeds the dipole dephasing time, in which situation the seed amplification and free induction decay play an essential role. These findings not only clarify the contentious key issue regarding to the amplification mechanism of N_2^+ lasing but also show the unique characteristics of ultrashort laser-induced amplification in a molecular ion system where both the microscopic and macroscopic quantum coherence might be present.

https://doi.org/10.1364/PRJ.434378

1. INTRODUCTION

Coherent laser sources, generated as a result of the strong laser–matter interaction, cover a broad electromagnetic spectrum from soft X-rays [1,2], visible light [3], to terahertz [4], and they are becoming powerful spectroscopic tools for exploring implications including ultrafast molecular imaging [5,6], remote sensing [7], and nonintrusive testing [8]. Particularly, the visible laser-like radiation from nitrogen molecular ions has received considerable attention in recent years due to its mysterious mechanisms and a broad interest in realizing highly sensitive remote detections with diversified Raman spectroscopies enabled by the new type of lasing [9–11]. Regarding its gain origins, the recent advances indicate that in addition to population inversion [12,13], multiple quantum coherences such as electronic [14–16], vibrational [17], and rotational coherences [18–20] can show some impact on the laser gain with a V-type three-level or a Λ-type multilevel model. These investigations have inspired some crucial thoughts associated with strong-field quantum optics such as photon retention [21], quantum erasing [22], and lasing without inversion [14].

Another fundamental issue that is still in hot debate concerning N_2^+ lasing is about its amplification mechanism. So far, at least two different amplification routes have been proposed. First, it is widely accepted that the collective emission of N_2^+ can be triggered at a relatively low gas pressure of pure nitrogen, i.e., triggered superradiance (TS) [23,24]. However, at a high gas pressure, it was found that the experimental observations can be well interpreted by the seed amplification (SA) physical picture [25–27]. Besides, it is also evidenced that the electronic coherence can be readily established via the existing coherent couplings [14–16], which possibly results in free induction decay (FID). Note that for the SA and FID, the excited molecular ions emit lights isolatedly. So these conflicting proposals raise a significant question: under what circumstances can the collective emission from molecular ions be initiated in strong laser fields?

To disentangle the complicated amplification process underlying N_2^+ lasing, we designed a cunning experiment to study the transformation of various amplification routes including seed amplification [28], triggered superradiance [29], and free induction decay [30] that may take place as weak ultra-

short laser propagates in an intense femtosecond laser-fabricated N_2^+ gain system. The decisive parameters describing the FID and TS processes are the dipole dephasing time T_2 and the characteristic damping time T_R of a collective system [31], respectively. The former and the latter are correspondingly related to the electronic coherence and macroscopic quantum coherence. Therefore, the amplification procedures can be controlled by finely monitoring the ratio of these two time-related quantities, permitting us to find the boundary conditions for observing collective radiations in molecular ions. The amplification flexibility realized by controlling various quantum coherences with ultrafast laser techniques is of particular significance for future applications in terms of quantum information storage and computation, which can currently only be realized in ultracold surroundings.

2. EXPERIMENTAL SETUP

The experimental configuration is schematically illustrated in Fig. 1(a). A commercial Ti:sapphire laser system working at a repetition rate of 1 kHz delivers laser pulses with duration 35 fs, the maximum energy 4 mJ, and the central wavelength at 795 nm. The output laser pulse was divided into three parts with two beam splitters. One, with energy of 2.2 mJ, was used as the pump, whose polarization was first tailored by a multiple half-wave plate (MHWP) with an order of $n = 11$. θ represents the angle between the initial laser polarization direction of the pump and the fast optical axis of the MHWP. The resulting pump polarization after the MHWP is that the rear and the front parts are linearly polarized yet mutually perpendicular, while the middle is a time-varying linear polarization [32,33]. A typical such polarization is depicted in the beam path. The second beam, with energy of 1 mJ, acted as the seed pulse after frequency doubling with a 0.3 mm thick β-barium-borate crystal. Considering the measured seed energy ~1 nJ, pulse duration ~120 fs, and incident beam diameter ~5 mm, the maximum seed intensity is estimated at 3×10^8 W/cm^2 under the current focusing conditions assuming a linear propagation. The polarization direction of the seed pulse was controlled with a zeroth-order half-wave plate at 397 nm. The time interval between the pump and seed pulses was controlled by a motorized translation stage with a resolution of 670 as. The pump and seed pulses were combined with a dichromatic mirror, and then they were focused with an $f = 30$ cm lens into a gas chamber filled with nitrogen at the pressure of 200 mbar. The generated forward lasing signals after being collimated by an $f = 25$ cm lens and filtered were collected with a grating spectrometer (Andor, 500i).

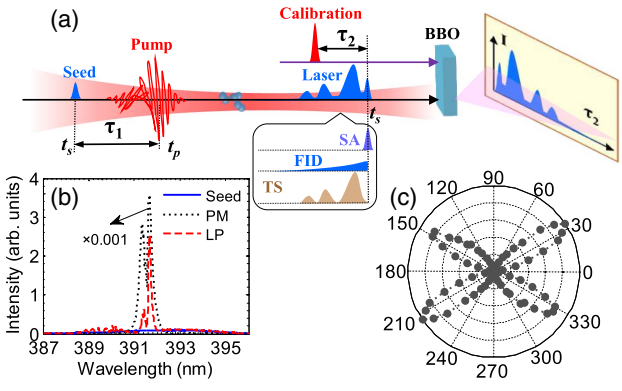

Fig. 1. (a) Schematic diagram of the pump-seed setup. A typical time profile of N_2^+ lasing amplified by different mechanisms is plotted. More details can be referred in the main text. (b) The typical N_2^+ lasing spectra measured under the pumping of the LP and PM pulses. (c) The dependence of the 391 nm lasing signal intensity on the angle θ.

A schematic plot of the time profiles of N_2^+ lasing induced by different mechanisms of SA, FID, and TS is shown in Fig. 1(a). When it was needed to calibrate the time profiles of the generated N_2^+ lasing, the third 795 nm pulse with energy of 0.4 mJ and the forward 391 nm lasing were simultaneously impinged on a 0.8 mm thick β-barium-borate crystal to produce sum frequency at ~262 nm by the cross correlation. To maximize the sum frequency signal, the polarization direction of the calibrating pulse was optimized with a second half-wave plate. This method is effective in sense that the time duration of the measured pulse is a few orders longer than that of the 795 nm femtosecond laser.

3. RESULTS

A typical 391 nm N_2^+ lasing [the electronic transition can be assigned to be $B^2\Sigma_u^+(\nu'' = 0) \rightarrow X^2\Sigma_g^+(\nu = 0)$] spectrum at the pump-seed delay of ~0.6 ps is plotted in Fig. 1(b). The seed intensity in this case is estimated at 2×10^7 W/cm^2, considering a linear focusing. The black dotted curve therein shows the strongest lasing signal obtained when the MHWP is rotated at $\theta = 32°$ as indicated in Fig. 1(c). We refer the corresponding pump laser (i.e., $\theta = 32°$) as the polarization-modulated (PM) pulse in the following. Apparently, the maximum lasing signal can be 3 orders stronger than that (the red dashed curve) produced with a linearly polarized (LP) laser pulse when the MHWP is adjusted to be $\theta = 0°$, which is consistent with previous experimental observations [32–34]. Of note, the central wavelength of the seed pulse is deliberately switched around 391 nm to induce SA efficiently as marked by the blue curve. Figure 1(c) shows the lasing signal intensity as a function of the angle θ. Clearly, the strongest lasing signal is achieved at $\theta = 32°$, and the minimum appears at $\theta = 0°$, which can be ascribed to the enhanced population inversion between the electronic states of $B^2\Sigma_u^+$ and $X^2\Sigma_g^+$ of N_2^+ in the PM laser field by favoring the optimization of the ionization and coupling processes comparing to the case of the LP excitation [32–34].

Figure 2 shows the normalized lasing intensities as a function of the seed intensity under the circumstance of the LP (circles) and PM (squares) laser excitation. The delay between the pump and seed pulses was fixed at ~0.6 ps in these cases. In the case of the LP laser excitation, the lasing signal grows linearly with the increasing seed intensity. However, under the pumping of the PM laser, the lasing signal first shows a sharp increase with the increment of seed intensity and then reaches saturation. The cyan and black dashed curves in Fig. 2 are the corresponding fitting curves by the superradiant and linear amplification theory, respectively. The fitting equation $\Theta = 2\arctan[\exp(T_w/T_R)\tan(\vartheta/2)]$ described with the superradiant theory can be found in Ref. [35], where ϑ, Θ

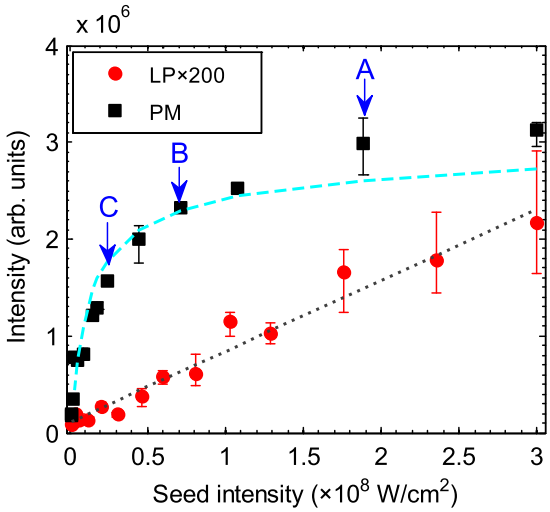

Fig. 2. N_2^+ lasing signal as a function of the seed intensity for the cases of the LP and PM ($\theta = 32°$) laser excitation. The signal intensity in the case of LP has been multiplied a factor of 200 for a direct comparison.

are the input and the output laser pulse area, respectively, and T_w is the time duration of superradiance. The fitting parameter $T_w/T_R = 4$ is basically consistent with the experimental result in Fig. 3(b).

To further determine the different properties of the generated 391 nm lasing for the cases of the LP and PM pulses, we measured their time profiles by the cross-correlation method [23]. Figures 3(a) and 3(b) separately show the recorded time profiles of the sum frequency signal at 262 nm after removing the input seed effect for the LP and PM laser pulses in each measurement. Therefore, the sum frequency signals can reflect the time structures of the N_2^+ lasing. Seed A, seed B, and seed C correspond to the seed intensities depicted by the arrows in the Fig. 2. The pink curve is given to show the seed time width for reference, which is obtained by blocking the pump pulse. In the left panel, it can be clearly seen that in the case of the LP laser, the main peak of the N_2^+ lasing appears at the falling edge of the seed time duration, and the signal lasts for 1.3 ps for a strong seed A. For the weak seeds B and C, the sum frequency signals are relatively small yet with a long tail. It is noted that the amplification efficiency of these two cases is basically a constant. We ascribed this to the insensitive amplification in a small-gain case. On contrary, for the case of the PM laser, the main peaks of the sum frequency signals for seeds A, B, and C no longer emerge within the seed pulse and are apparently delayed in time with respect to the seed pulse as implied in Fig. 3(b). Besides, it can also be inferred that the retarded time T_D (defined as the time interval between the peak of the seed pulse and that of the output sum frequency signal) is greatly reduced with the increment of the seed intensity. Figure 3(c) presents the relation of the retarded time T_D (red stars) to the seed intensity for the PM case, which in essence is the TS process as we demonstrated below. The dashed curve is the corresponding fitting given by the equation $T_D = \frac{1}{4} T_R |\ln(\frac{\vartheta}{2\pi})|^2$ [35]. The qualitative agreement validates the superradiance mechanism under the conditions.

To interpret the experimental observations, we first simulate the formation of N_2^+ system under the irradiation of the pump laser using the recently proposed ionization-coupling model encapsulating the strong-field transient ionization and coherent coupling processes [36,37]. The initial ground state N_2 exposed to the pump laser field can be ionized to the electronic states of $X^2\Sigma_g^+$ (X), $A^2\Pi_u$ (A), and $B^2\Sigma_u^+$ (B) of N_2^+ by direct tunneling ionization, and the population transfer among these ionic states occurs upon transient ionization. Of note, the doubly degenerate states of $A^2\Pi_u$ are included in our simulations. The adopted pump laser parameters: the time duration $\tau_p = 40$ fs, the peak intensity $I = 3.5 \times 10^{14}$ W/cm^2, and the central wavelength $\lambda = 800$ nm, are close to the experiments. For the cases of the LP and PM lasers, the calculated ionic population distribution is averaged on the angle $\alpha = 0°$, 30°, 45°, 60°, and 90°, where α represents the angle between the pump laser polarization and the molecular axis. Similar to our previous descriptions [36,37], the ionic density matrix ρ^+ can be expressed as

$$\frac{d\rho^+}{dt} = -\frac{i}{\hbar}[H, \rho^+] + \left(\frac{d\rho^+_{i\nu k}}{dt}\right)_{ion} + \left(\frac{d\rho^+}{dt}\right)_{coll}, \quad (1)$$

where i, ν, and k denote the electronic, vibrational, and rotational states of N_2^+, respectively. The middle term on the right side of Eq. (1) represents the transient ionization injection

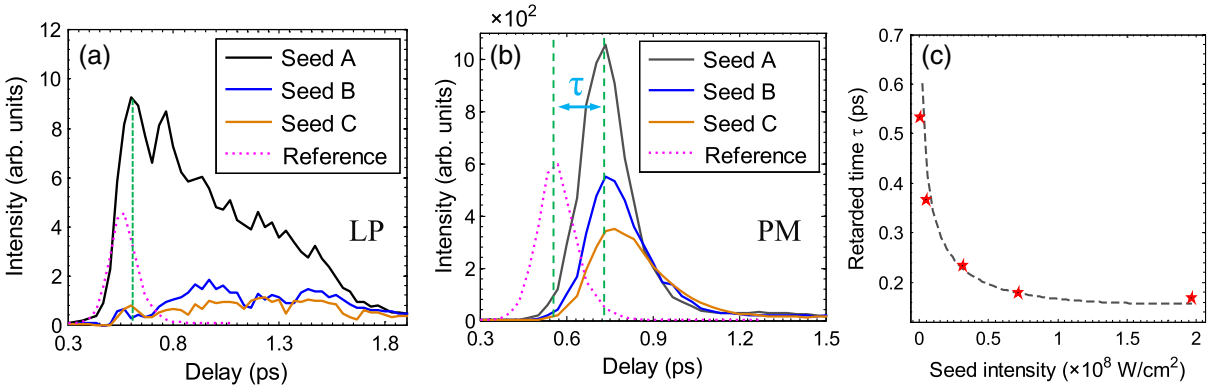

Fig. 3. Measured time structures of N_2^+ lasing under the triggering of various seed intensities for the pumping of the (a) LP and (b) PM laser. The longitudinal axis in these two cases is normalized by the same value. (c) The retarded time τ as a function of the seed intensity for the PM laser.

within the pump laser field [18,37]. It deserves mentioning that the collision-induced decay is introduced on the right side of Eq. (1), which causes a time-dependent population inversion between the states of $B(\nu''=0)$ and $X(\nu=0)$ after the passage of the pump laser. H is the ionic Hamiltonian:

$$H=\begin{bmatrix} E_B^{\nu''k} & 0 & d_{BX}^{\nu''\nu}\cdot\varepsilon_p \\ 0 & E_A^{\nu'k} & d_{AX}^{\nu'\nu}\cdot\varepsilon_p \\ d_{BX}^{\nu''\nu}\cdot\varepsilon_p & d_{AX}^{\nu'\nu}\cdot\varepsilon_p & E_X^{\nu k} \end{bmatrix}, \tag{2}$$

where ε_p is the electric field of the pump laser, $E_i^{\nu k}$ is the diagonal matrix composed of the eigenenergy value of each state, and $d_{ij}^{\nu'\nu}$ is the transition dipole moment matrix between the electronic-vibrational states. $i,j=X,A,B$; $\nu,\nu',\nu''=0$–4; $k=0$–49.

Next, the time-delayed seed pulse interacts with the prepared ionic system. As the seed pulse is quite weak, and its central wavelength is around 391 nm, we employ the following Maxwell–Bloch equation combining with the density matrix formalism to simulate its propagation based on a two-level system [i.e., $B(\nu''=0)$ and $X(\nu=0)$]:

$$\left(c\frac{\partial}{\partial z}+\frac{\partial}{\partial t}\right)E=i\Omega_0\sigma_{BX}, \tag{3}$$

$$\frac{\mathrm{d}\rho}{\mathrm{d}t}=-\frac{i}{\hbar}[H_{\mathrm{two}},\rho]+\left(\frac{\mathrm{d}\rho}{\mathrm{d}t}\right)_{\mathrm{coll}}, \tag{4}$$

where E is the Gaussian envelope of the propagating pulse with electric field $\varepsilon(t)=\frac{1}{2}E(t)e^{i(kz-\omega t)}$ and $\Omega_0=\omega N d_{BX}^{00}/\varepsilon_0$ is the propagating constant. ω is the seed light frequency. $N=8\times10^{16}\,\mathrm{cm}^{-3}$ is the population density of N_2^+; d_{BX}^{00} is the transition dipole moment between $B(\nu''=0)$ and $X(\nu=0)$. σ_{BX} is the slow-varying amplitude of the coherence $\rho_{BX}=\frac{1}{2}\sigma_{BX}e^{i(kz-\omega t)}$. ρ is the density matrix of the two-level system. H_{two} is the Hamiltonian of the two-level system:

$$H_{\mathrm{two}}=\begin{bmatrix} E_B^0 & d_{BX}^{00}\varepsilon(t) \\ d_{BX}^{00}\varepsilon(t) & E_X^0 \end{bmatrix}. \tag{5}$$

The second term on the right of Eq. (3) is the decay term brought by collisions:

$$\left(\frac{\mathrm{d}\rho_{BB}}{\mathrm{d}t}\right)_{\mathrm{coll}}=-\frac{\rho_{BB}}{T_1};\qquad \left(\frac{\mathrm{d}\rho_{ij}}{\mathrm{d}t}\right)_{\mathrm{coll}}=-\frac{\rho_{ij}}{T_2},\qquad i\neq j, \tag{6}$$

where $i,j=X,B$. T_1 and T_2, signifying depopulation and dephasing, are set to be 2.5 ps. Besides, the matrix element ρ_{XX} in Eq. (4) is calculated by $\dot{\rho}_{XX}=-i\hbar^{-1}[d_{BX}^{00}\varepsilon(t)\rho_{BX}+\mathrm{c.c.}]$, while neglecting the decay term, since the electronic state $X(\nu=0)$ is the ground state of N_2^+. In the simulation, the duration of the seed pulse is ~120 fs. The gain medium length $L=0.9$ cm. It should be noted that at the arrival of the seed pulse the established population inversion $Z=\rho_{BB}-\rho_{XX}$ is different for the LP and PM cases, which are 1.4×10^{-2} and 8.8×10^{-2} for the pump-seed delay of ~0.6 ps, respectively. The amount of population inversion significantly influences the amplification of N_2^+ lasing.

Figures 4(a) and 4(b) show the calculated time profiles of 391 nm lasing after subtracting the input seed laser for the LP and PM pumping, respectively. It can be clearly seen that

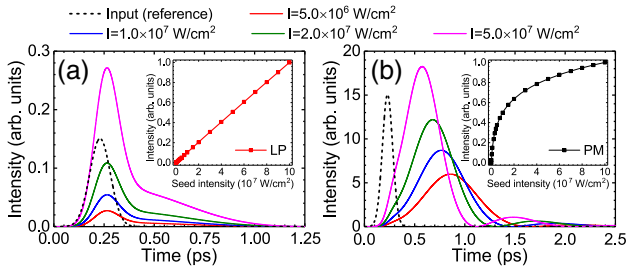

Fig. 4. Simulated time profiles of 391 nm lasing at various seed intensities under excitation of the (a) LP and (b) PM laser. The insets show the corresponding lasing intensity as a function of the seed intensity for these two situations.

for the LP case, the main peaks of the amplified laser pulses are observed at the falling edge of the seed pulse, which can be attributed to the coexistence of the population inversion and electronic coherence, and their intensities exhibit a linear growth with the seed intensity as displayed in the inset of Fig. 4(a). Besides, after the passage of the seed pulse, an amplified long tail is also observed, which is in fact closely associated with the dephasing time T_2. As shown in Fig. 4(b), the peaks of the amplified 391 nm lasing are postponed relative to the seed for the PM laser, and the retarded time τ is up to the seed intensity. The nonlinear dependence of the integrating lasing intensity on the seed intensity is also plotted as an inset. Therefore, with the current model, the simulated results agree well with the measured results shown in Figs. 2 and 3.

4. DISCUSSION

The amplification process of N_2^+ lasing is closely related to its origin of gain. First of all, since the population inversion between the states of $B(\nu''=0)$ and $X(\nu=0)$ is met by both the LP and PM lasers, the SA can be induced under a resonant excitation. Note that the amplification within the seed duration has escaped from observations in previous experiments despite SA having been initially proposed [25–27]. The reason behind this is that the seed spectrum has been shifted away from resonance in most prior investigations, and the time window for SA is usually too short to produce a discernible signal [23,24]. For the sake of offering direct evidence for SA, we tried to promote the ratio of SA by injecting a 391 nm seed with a relatively large pulse area ϑ. Second, a net gain can also be attained by preparing quantum coherence, giving rise to a post-seed-pulse amplification. Herein, two types of coherent amplifications should be distinguished [38], i.e., FID and TS. The indispensable condition for the FID is the electronic quantum coherence σ_{BX}, which is enabled by the resonant seed pulse in our cases. It is not difficult to deduce that under a weak excitation, the amplitude of the electronic coherence σ_{BX} is approximately proportional to the seed pulse area ϑ for a two-level system [39]. The FID signal typically decays with the loss of coherence determined by the dephasing time T_2. On the other hand, the TS differs from FID due to the collective emission of the individual quantum emitters that are bonded by a weak field [38]. The systematic gain can be defined as $\beta=T_2/T_{\mathrm{R}}$, where the

value of T_R is inversely proportional to the population inversion density [31,40].

Recall that under a weak triggering the condition for generating superradiant amplification is $T_D < T_2$ [41], where the retarded delay $T_D = \frac{1}{4} T_R |\ln(\frac{\vartheta}{2\pi})|^2$ [31,41], or equivalently, $\beta > \frac{1}{4}|\ln(\frac{\vartheta}{2\pi})|^2$. Therefore, for the PM laser, the TS can be easily initiated for the range of seed intensity of $I_{seed} > 6\ W/cm^2$ due to $\beta = 33$. The results presented by the black squares in Fig. 2 and those in Fig. 3(b) can be well fitted by the superradiant theory, confirming that TS is the primary amplification mechanism for PM laser excitation. However, for LP pumping, the evaluated β is 5, and thus the collective emission of ions solely occurs for the seed intensity of $I_{seed} > 10^7\ W/cm^2$ in principle. We ascribe the amplification during and after the seed pulse in Fig. 3(a) to SA and FID, respectively, which explains the linear dependence of the lasing intensity on the seed intensity as marked by the red circles in Fig. 2. It deserves mention that for a limiting case of a strong seed pulse, a fierce competition between the SA and TS exists within the seed duration, and a dynamic superradiant theory is required.

Finally, we would like to point out that the three abovementioned amplification mechanisms are in fact mutually influenced. For example, the SA process could deplete a portion of the population inversion, showing a great impact on the follow-up FID and TS. Additionally, the dephasing time T_2, determining the ending time of FID, is also critical for TS. In Fig. 5, we show the simulated amplification ratio $(I - I_0)/I_0$ on a log scale as a function of β and ϑ, where I and I_0 are respectively the output lasing intensity and input seed intensity. The seed intensity is limited to the value of $I_{seed} < 2 \times 10^8\ W/cm^2$. The red and black curves are the corresponding gains similar to the experimental conditions in Fig. 2, and seeds A, B, and C for experimental measurements are marked by the dots. It can be clearly seen that for $\beta < 12$, the output lasing signals obviously show a nearly linear dependence on the seed pulse area ϑ, indicating that SA and FID prevail over TS in this regime. Nevertheless, a nonlinear amplification appears for $\beta > 12$, and TS gradually becomes the dominating mechanism with the further increment of β. These results indicate that the collective emission of molecular ions in strong laser fields can be controlled by manipulating the gain factor β, i.e., T_2 or T_R. We noticed that the control of the collective emission was achieved by changing the dipole dephasing time T_2 in a KCl crystal [42].

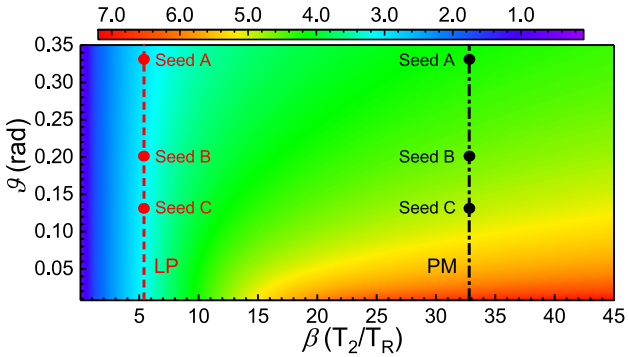

Fig. 5. Calculated lasing signal $(I - I_0)/I_0$ on a log scale as a function of β and the seed pulse area ϑ with $T_{1,2} = 2.5$ ps. The red and black dashed lines correspond to the amplification similar to the case of the LP and PM laser in Fig. 2.

To summarize, we systematically investigated the amplification mechanism of N_2^+ lasing and found that a time-sequential amplification composed of SA, TS, and FID may happen in such a population-inverted quantum system. It is revealed that the ratio of these three amplification mechanisms can be readily switched by the experimental parameters such as ϑ and β, by which the requirement for observing the collective emission of molecular ions in a strong laser field is gained. Besides, our results also suggest that the molecular ions generated by transient ionization and coherent couplings can be ideal candidates for performing investigations on strong-field quantum optics. These findings clearly verify the distinctions and show the advantages of amplification in femtosecond laser-prepared ionic systems, compared to that induced by conventional nanosecond lasers.

Funding. Major Research Plan (91850201); National Key Research and Development Program of China (2019YFA0307703); National Natural Science Foundation of China (12074063; 12064009; 12034013; 11874066; 11822410); Program of Shanghai Academic Research Leader (20XD1424200); Hunan Provincial Innovation Foundation for Postgraduate (CX20200035).

Disclosures. The authors declare no conflicts of interest.

Data Availability. The data that support the findings of this study are available from the corresponding author upon reasonable request.

†These authors contributed equally to this paper.

REFERENCES

1. T. Popmintchev, M. Chen, D. Popmintchev, P. Arpin, S. Brown, S. Ališauskas, G. Andriukaitis, T. Balčiunas, O. Mücke, A. Pugzlys, A. Baltuška, B. Shim, S. Schrauth, A. Gaeta, C. García, L. Plaja, A. Becker, A. Becker, M. Murnane, and H. Kapteyn, "Bright coherent ultrahigh harmonics in the keV X-ray regime from mid-infrared femtosecond lasers," Science **336**, 1287–1291 (2012).
2. L. He, G. Yuan, K. Wang, W. Hua, C. Yu, and C. Jin, "Optimization of temporal gate by two-color chirped lasers for the generation of isolated attosecond pulse in soft X rays," Photon. Res. **7**, 1407–1415 (2019).
3. J. Yao, B. Zeng, H. Xu, G. Li, W. Chu, J. Ni, H. Zhang, S. L. Chin, Y. Cheng, and Z. Xu, "High-brightness switchable multiwavelength remote laser in air," Phys. Rev. A **84**, 051802 (2011).
4. J. Zhao, W. Liu, S. Li, D. Lu, Y. Zhhang, Y. Peng, Y. Zhu, and S. Zhuang, "Clue to a thorough understanding of terahertz pulse generation by femtosecond laser filamentation," Photon. Res. **6**, 296–306 (2018).
5. C. Bostedt, E. Eremina, D. Rupp, M. Adolph, H. Thomas, M. Hoener, A. R. B. de Castro, J. Tiggesbäumker, K.-H. Meiwes-Broer, T. Laarmann, H. Wabnitz, E. Plönjes, R. Treusch, J. R. Schneider, and T. Möller, "Ultrafast X-ray scattering of xenon nanoparticles: imaging transient states of matter," Phys. Rev. Lett. **108**, 093401 (2012).
6. A. S. Ashik, C. F. O'Donnell, S. Chaitanya Kumar, M. Ebrahim-Zadeh, P. Tidemand-Lichtenberg, and C. Pedersen, "Mid-infrared upconver-

sion imaging using femtosecond pulses," Photon. Res. **7**, 783–791 (2019).
7. H. Xu, Y. Cheng, S.-L. Chin, and H.-B. Sun, "Femtosecond laser ionization and fragmentation of molecules for environmental sensing," Laser Photon. Rev. **9**, 275–293 (2015).
8. S. Chen, Z. Feng, J. Li, W. Tan, L.-H. Du, J. Cai, Y. Ma, K. He, H. Ding, Z.-H. Zhai, Z. Li, C.-W. Qiu, X.-C. Zhang, and L. Zhu, "Ghost spintronic THz-emitter-array microscope," Light Sci. Appl. **9**, 99 (2020).
9. J. Ni, W. Chu, H. Zhang, B. Zeng, J. Yao, L. Qiao, G. Li, C. Jing, H. Xie, H. Xu, Y. Cheng, and Z. Xu, "Impulsive rotational Raman scattering of N_2 by a remote 'air lase' in femtosecond laser filament," Opt. Lett. **39**, 2250–2253 (2014).
10. X. Zhao, S. Nolte, and R. Ackermann, "Lasing of N_2^+ induced by filamentation in air as a probe for femtosecond coherent anti-Stokes Raman scattering," Opt. Lett. **45**, 3661–3664 (2020).
11. G. Li, H. Xie, Q. Zhang, H. Lei, X. Zhou, X. Wang, Z. Chen, and Z. Zhao, "Enhanced resonant vibrational Raman scattering of N_2^+ induced by self-seeding ionic lasers created in polarization-modulated intense laser fields," Opt. Lett. **45**, 5616–5619 (2020).
12. H. Xu, E. Lötstedt, A. Iwasaki, and K. Yamanouchi, "Sub-10-fs population inversion in N_2^+ in air lasing through multiple state coupling," Nat. Commun. **6**, 8347 (2015).
13. J. Yao, S. Jiang, W. Chu, B. Zeng, C. Wu, R. Lu, Z. Li, H. Xie, G. Li, C. Yu, Z. Wang, H. Jiang, Q. Gong, and Y. Cheng, "Population redistribution among multiple electronic states of molecular nitrogen ions in strong laser fields," Phys. Rev. Lett. **116**, 143007 (2016).
14. A. Mysyrowicz, R. Danylo, A. Houard, V. Tikhonchuk, X. Zhang, Z. Fan, Q. Liang, S. Zhuang, L. Yuan, and Y. Liu, "Lasing without population inversion in N_2^+," APL Photon. **4**, 110807 (2019).
15. A. Zhang, Q. Liang, M. Lei, L. Yuan, Y. Liu, Z. Fan, X. Zhang, S. Zhuang, C. Wu, Q. Gong, and H. Jiang, "Coherent modulation of superradiance from nitrogen ions pumped with femtosecond pulses," Opt. Express **27**, 12638–12646 (2019).
16. J. Chen, J. Yao, H. Zhang, Z. Liu, B. Xu, W. Chu, L. Qiao, Z. Wang, J. Fatome, O. Faucher, C. Wu, and Y. Cheng, "Electronic-coherence-mediated molecular nitrogen-ion lasing in a strong laser field," Phys. Rev. A **100**, 031402 (2019).
17. B. Xu, J. Yao, Y. Wan, J. Chen, Z. Liu, F. Zhang, W. Chu, and Y. Cheng, "Vibrational Raman scattering from coherently excited molecular ions in a strong laser field," Opt. Express **27**, 018262 (2019).
18. H. Xie, H. Lei, G. Li, Q. Zhang, X. Wang, J. Zhao, Z. Chen, J. Yao, Y. Cheng, and Z. Zhao, "Role of rotational coherence in femtosecond-pulse-driven nitrogen ion lasing," Phys. Rev. Res. **2**, 023329 (2020).
19. M. Richter, M. Lytova, F. Morales, S. Haessler, O. Smirnova, M. Spanner, and M. Ivanov, "Rotational quantum beat lasing without inversion," Optica **7**, 586–592 (2020).
20. L. Arissian, B. Kamer, A. Rastegari, D. Villeneuve, and J. Diels, "Transient gain from N_2^+ in light filaments," Phys. Rev. A **98**, 053438 (2018).
21. J. Yao, L. Wang, J. Chen, Y. Wan, Z. Zhang, F. Zhang, L. Qiao, S. Yu, B. Fu, Z. Zhao, C. Wu, V. Yakovlev, L. Yuan, X. Chen, and Y. Cheng, "Photon retention in coherently excited nitrogen ions," Sci. Bull. **66**, 1511–1517 (2021).
22. R. Danylo, G. Lambert, Y. Liu, V. Tikhonchuk, A. Houard, and A. Mysyrowicz, "Quantum erasing of laser emission in N_2^+," Opt. Lett. **45**, 4670–4673 (2020).
23. G. Li, C. Jing, B. Zeng, H. Xie, J. Yao, W. Chu, J. Ni, H. Zhang, H. Xu, Y. Cheng, and Z. Xu, "Signature of superradiance from a nitrogen-gas plasma channel produced by strong-field ionization," Phys. Rev. A **89**, 033833 (2014).
24. Y. Liu, P. Ding, G. Lambert, A. Houard, V. Tikhonchuk, and A. Mysyrowicz, "Recollision-induced superradiance of ionized nitrogen molecules," Phys. Rev. Lett. **115**, 133203 (2015).
25. H. Xu, E. Lötstedt, T. Ando, A. Iwasaki, and K. Yamanouchi, "Alignment-dependent population inversion in N_2^+ in intense few-cycle laser fields," Phys. Rev. A **96**, 041401 (2017).
26. J. Yao, G. Li, C. Jing, B. Zeng, W. Chu, J. Ni, H. Zhang, H. Xie, C. Zhang, H. Li, H. Xu, S. Chin, Y. Cheng, and Z. Xu, "Remote creation of coherent emissions in air with two-color ultrafast laser pulses," New J. Phys. **15**, 023046 (2013).
27. W. Zheng, Z. Miao, L. Zhang, Y. Wang, C. Dai, A. Zhang, H. Jiang, Q. Gong, and C. Wu, "Enhanced coherent emission from ionized nitrogen molecules by femtosecond laser pulses," J. Phys. Chem. Lett. **10**, 6598–6603 (2019).
28. T. Maiman, "Stimulated optical radiation in ruby," Nature **187**, 493–494 (1960).
29. N. Carlson, D. Jackson, and A. Schawlow, "Superradiance triggering spectroscopy," Opt. Commun. **32**, 350–354 (1980).
30. R. G. Brewer and R. L. Shoemaker, "Optical free induction decay," Phys. Rev. A **6**, 2001–2007 (1976).
31. J. MacGillivray and M. Feld, "Theory of superradiance in an extended, optically thick medium," Phys. Rev. A **14**, 1169–1189 (1976).
32. H. Li, M. Hou, H. Zang, Y. Fu, E. Lötstedt, T. Ando, A. Iwasaki, K. Yamanouchi, and H. Xu, "Significant enhancement of N_2^+ lasing by polarization-modulated ultrashort laser pulses," Phys. Rev. Lett. **122**, 013202 (2019).
33. H. Xie, Q. Zhang, G. Li, X. Wang, L. Wang, Z. Chen, H. Lei, and Z. Zhao, "Vibrational population transfer between electronic states of N_2^+ in polarization-modulated intense laser fields," Phys. Rev. A **100**, 053419 (2019).
34. H. Li, E. Lötstedt, H. Li, Y. Zhou, N. Dong, L. Deng, P. Lu, T. Ando, A. Iwasaki, Y. Fu, S. Wang, J. Wu, K. Yamanouchi, and H. Xu, "Giant enhancement of air lasing by complete population inversion in N_2^+," Phys. Rev. Lett. **125**, 053201 (2020).
35. M. Benedict, A. Ermolaev, V. Malyshev, I. Sokolov, and E. Trifonov, *Super-Radiance: Multiatomic Coherent Emission* (Institute of Physics, 1996).
36. Q. Zhang, H. Xie, G. Li, X. Wang, H. Lei, J. Zhao, Z. Chen, J. Yao, Y. Cheng, and Z. Zhao, "Sub-cycle coherent control of ionic dynamics via transient ionization injection," Commun. Phys. **3**, 50 (2020).
37. H. Lei, G. Li, H. Xie, Q. Zhang, X. Wang, J. Zhao, Z. Chen, and Z. Zhao, "Mechanism and control of rotational coherence in femtosecond laser-driven N_2^+," Opt. Express **28**, 22829–22843 (2020).
38. R. Jodoin and L. Mandel, "Superradiance and optical free induction," Phys. Rev. A **10**, 1898–1903 (1974).
39. M. Scully and M. Zubairy, *Quantum Optics* (Cambridge University, 1997).
40. M. Houde, F. Rajabi, B. M. Gaensler, A. Mathews, and V. Tranchant, "Triggered superradiance and fast radio bursts," Mon. Not. R. Astron. Soc. **482**, 5492–5499 (2019).
41. J. Maki, M. Malcuit, M. Raymer, and R. Boyd, "Influence of collisional dephasing processes on superfluorescence," Phys. Rev. A **40**, 5135–5142 (1989).
42. M. Malcuit, J. Maki, D. Simkin, and R. Boyd, "Transition from superfluorescence to amplified spontaneous emission," Phys. Rev. Lett. **59**, 1189–1192 (1987).